New Zealand Journal of Marine and Freshwater Research

ISSN: 0028-8330 (Print) 1175-8805 (Online) Journal homepage: https://www.tandfonline.com/loi/tnzm20

The Fiordland Current, southwest New Zealand: mean, variability, and trends

Mitchell Chandler, Melissa Bowen & Robert Owain Smith

To cite this article: Mitchell Chandler, Melissa Bowen & Robert Owain Smith (2019): The Fiordland Current, southwest New Zealand: mean, variability, and trends, New Zealand Journal of Marine and Freshwater Research, DOI: 10.1080/00288330.2019.1629467

To link to this article: https://doi.org/10.1080/00288330.2019.1629467

Published online: 16 Jun 2019.

NEW ZEALAND JOURNAL OF MARINE AND FRESHWATER RESEARCH
https://doi.org/10.1080/00288330.2019.1629467

Taylor & Francis
Taylor & Francis Group

RESEARCH ARTICLE

The Fiordland Current, southwest New Zealand: mean, variability, and trends

Mitchell Chandler[a], Melissa Bowen[a] and Robert Owain Smith[b]

[a]School of Environment, University of Auckland, Auckland, New Zealand; [b]Department of Marine Science, University of Otago, Dunedin, New Zealand

ABSTRACT

The mean, interannual variability, decadal variability, and longer-term trends in the across-track geostrophic velocity of the poleward-flowing boundary current along the Fiordland coast (the Fiordland Current, FC) are examined over the altimeter record (September 1992–May 2017). In the mean, the FC is southwestward, with stronger velocities in an inner current near the coast and weaker velocities in an outer current further offshore. Examination of the alongshore momentum balance suggests that the mean flow is driven by a poleward downsloping alongshore pressure gradient. At interannual time-scales, variability in the FC was correlated with the alongshore wind stress, indicating that an equatorward (poleward) wind stress drives an equatorward (poleward) velocity anomaly. At decadal time-scales, variability in the FC was correlated with the South Pacific wind stress curl, indicating that as the wind stress curl increases (decreases) the poleward flow in the FC weakens (strengthens), consistent with the response of a traditional eastern boundary current. Long-term trends show a weakening outer current and strengthening inner current. Increasing flow in the inner current may result in increased transport of subtropical water around southern New Zealand.

ARTICLE HISTORY
Received 28 March 2019
Accepted 5 June 2019

KEYWORDS
Fiordland Current; Southland Current; Westland Current; eastern boundary Current; wind-driven ocean circulation; ocean satellite altimetry

Introduction

The boundary current off the west coast of Fiordland, southwest New Zealand, is a narrow, poleward-flowing current located close to the coast (Heath 1973). It likely originates around 41–44°S, where the weak (c. 3 Sv, 1 Sv = 10^6 m^3 s^{-1}) eastward geostrophic transport in the vicinity of the Subtropical Front (STF) (Stramma et al. 1995) separates into a northward-flowing current (the Westland Current, WC) and a southward-flowing current (Figure 1) (Heath 1973, 1975; Stanton 1976; Heath 1982, 1985; Stanton and Moore 1992; Ridgway and Dunn 2003; Chiswell et al. 2015). The current provides a pathway for the flow of subtropical water (STW) out of the Tasman Sea, and is part of the anticlockwise flow around southern New Zealand (Brodie 1960; Heath 1973, 1975; Chiswell et al. 2015).

The extent to which this current is connected to the Southland Current (SC) on the east coast of the South Island is not entirely clear, as the SC has historically referred to two

CONTACT Mitchell Chandler mcha867@aucklanduni.ac.nz

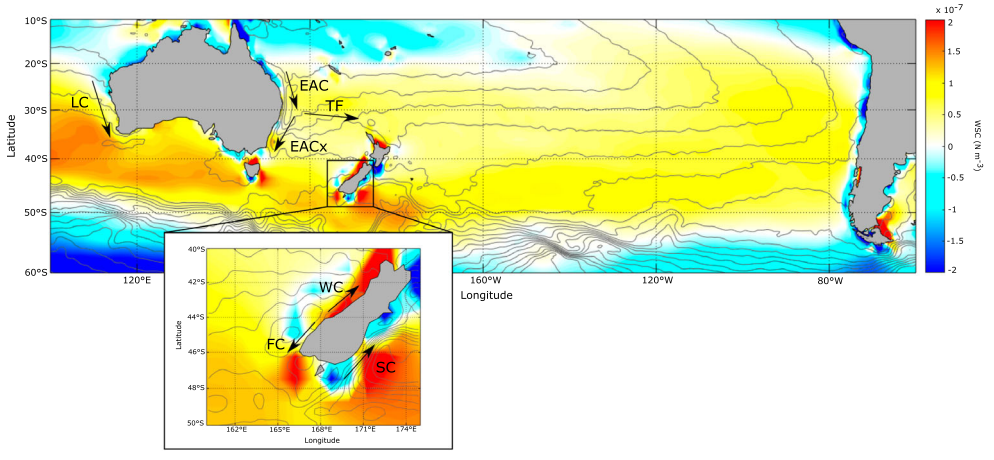

Figure 1. Schematic of the main currents referred to in the text. Currents are; Leeuwin Current (LC), East Australian Current (EAC), East Australian Current extension (EACx), Tasman Front (TF), Westland Current (WC), Fiordland Current (FC), Southland Current (SC). Colours are the wind stress curl (WSC, N m^{-3}) of the mean wind between 1993–2017. Grey contours are the mean dynamic topography for 1993–2012.

different geographic extents of flow. In earlier studies of New Zealand coastal currents, the STW flowing southwestward along the Fiordland coast, eastwards around southern New Zealand, and then northeastward up the east coast of the South Island was considered the SC (Brodie 1960; Heath 1975). Stanton (1976), Butler et al. (1992), Stanton and Moore (1992), and Hamilton (2006) also all referred to this southwestward flowing boundary current off the Fiordland coast as the SC. However, in more recent literature, the SC is usually considered to extend along the upper continental slope southeast of Stewart Island and flow northeastwards up the east coast of the South Island (Figure 1) (Chiswell 1996; Sutton 2003; Cortese et al. 2013; Chiswell et al. 2015; Stevens et al. 2019). To further complicate the region, a recent review (Stevens et al. 2019) appears to identify both the equatorward and poleward flowing currents along the South Island west coast as the WC. Therefore, to avoid any ambiguity in distinguishing between the current off the Fiordland coast that is the focus of this study and both the WC and the SC, it is proposed that the current off the Fiordland Coast be named the Fiordland Current (FC), and it will be referred to as such in this study.

It is thought that the FC is driven by a poleward pressure gradient that opposes the prevailing winds (Stanton 1976; Ridgway and Dunn 2003). Like the FC, the Leeuwin Current (LC) off the west coast of Australia is also a poleward-flowing eastern boundary current (EBC, Figure 1) driven by these same mechanisms (Godfrey and Ridgway 1985; Morrow and Birol 1998; Feng et al. 2003; Ridgway and Condie 2004; Feng et al. 2005). It has therefore been suggested that the FC may exhibit dynamics similar to the LC (Ridgway and Dunn 2003). However, little work has been conducted examining variability in the FC. Stanton (1976) believed that the component of the FC driven by the predominant westerly winds was not strong enough to reverse the southwestward flow of the geostrophic current. This was supported by Stanton and Moore (1992) who found that a southwestward geostrophic current was always present, although a northeastward

flowing coastal current developed under northeastward wind stress. Therefore the FC was not always found up against the coast, with the northeastward coastal current likely moving the core of the FC offshore. Cahill et al. (1991) also found, from moorings at roughly 60 m depth, that while the flow was generally poleward, equatorward velocities occasionally developed. Using one month of moored current meter data offshore of Milford Sound, Chiswell (1996) found that the southwestward flow reversed and became northeastward 36% of the time.

Variability in other boundary currents around New Zealand has received some attention. A model by Heath (1982) found that currents on the west coast continental shelf were predominantly driven by boundary forcing and local winds. Cahill et al. (1991) found that alongshore currents on the South Island west coast shelf were related to the alongshore wind stress through Cook Strait, which they believed was producing coastally trapped waves. They also found that alongshore wind stress along the west coast was producing alongshore currents. Sutton and Bowen (2011) found that variability in the flow offshore of the 1000 m isobath off the northwest coast of the North Island was largely geostrophic, while inshore variability was correlated to changes in wind stress. On the east coast of New Zealand, Chiswell (1996) found that, over seven months of data, variability in the SC was mainly driven by local winds. Fernandez et al. (2018) concluded that New Zealand's western boundary currents (WBCs) were highly variable with no significant trends over the 1993–2014 period. Little research has been carried out on El Nino-Southern Oscillation (ENSO) driven variability in New Zealand boundary currents; though studies have suggested ENSO can have an impact despite often inconsistent boundary current responses (e.g. Stanton 2001; Hopkins et al. 2010; Fernandez et al. 2018).

Changes in the large-scale wind field also impact on boundary currents in the southwest Pacific. Hill et al. (2011) found that decadal variability in the strength of the East Australian Current extension (EACx) and Tasman Front (TF) were related to decadal variability in the South Pacific wind stress curl (SPWSC), with maximum wind stress curl (WSC) associated with maximum poleward transport in the EACx. Fernandez et al. (2018) also found that the SPWSC showed a decadal signal over their 20-year (1993–2013) study period. Longer-term trends in the FC related to long-term changes in the SPWSC might also be expected. For example, the EACx extended further south over the c. 60-year (1944–2002) period examined by Ridgway (2007), resulting in increased sea-surface temperature (SST) and salinity to the east of Tasmania. This increased southward penetration of the East Australian Current (EAC) is believed to have been caused by a strengthening of the SPWSC over the last half century, which shifts the South Pacific subtropical gyre south and favours transport in the EACx over the TF (Cai 2006; Ridgway 2007; Roemmich et al. 2007; Hill et al. 2008, 2011; Shears and Bowen 2017).

Increased transport of STW around southern New Zealand, as anticipated under increased SPWSC, may lead to an increase in water temperatures to the south of New Zealand (Cortese et al. 2013; Shears and Bowen 2017) and a change in the proportion of STW being transported northward along the southeast coast of New Zealand via the SC, which transports predominantly subantarctic water (Sutton 2003). Changes in the southward transport of STW in the FC may also influence the position of the STF around southern New Zealand (Hamilton 2006; Smith et al. 2013). These changes may impact on the marine ecology of the region (Shears and Bowen 2017), as has been seen

to occur with increased southward penetration of the EAC (e.g. Ling et al. 2009; Fowler et al. 2018).

Despite the possible importance of the FC to the oceanography and marine ecosystems of southern New Zealand, little is known about its variability or long-term trends. Given the influence of both local and large-scale winds on other boundary currents in the region, it is expected that variability in the FC may be predominantly wind-driven. If the SPWSC is a key driver, a decadal signal in the FC may be present.

This paper uses sea-level anomaly (SLA) data from the Copernicus Marine Environment Monitoring Service (CMEMS) and mean dynamic topography (MDT) from Aviso+ to identify the mean, variability, and longer-term trends in the geostrophic velocity of the FC over the altimeter record (the last approximately 25 years). The across-track surface geostrophic velocities are compared to both local and regional winds, to the alongshore pressure gradient, and to the Southern Oscillation Index (SOI) to determine the extent to which these are related to variability in the FC. Data products and analysis are outlined in the Methods section, with the geostrophic velocities and outcomes of the analysis presented in the Results section. Relationships between these factors considered and the FC are commented on and possible drivers of the mean, variability, and trends in the FC are identified in the Discussion section. The Conclusion section summarises the main findings.

Methods

Sea-level anomaly (SLA) and mean dynamic topography

Data

Unfiltered, 1 Hz (6.19 km), along-track, delayed-time SLA data between 25 September 1992–15 May 2017, produced and distributed by CMEMS (http://www.marine.copernicus.eu), were used in this study. Data were collected by the Topex/Poseidon, Jason-1, OSTM/Jason-2, and Jason-3 satellite altimeters passing over the same track every 9.9 days. SLAs are referenced to the 1993–2012 mean and the standard corrections and quality control have been applied (Taburet 2018).

SLA measurements from track 36 (Figure 2) were used to study the FC. The closest altimeter measurement to the coast was approximately 11 km offshore along the altimeter track, and the furthest altimeter measurement considered was approximately 92 km offshore along the altimeter track (hereafter referred to as offshore). In total, 14 altimeter measurement locations along the track were considered.

Approximately 10% of data points were missing. Missing values were infilled through extrapolation and interpolation of smaller gaps in space, and interpolation of larger gaps in time. For the spatial extrapolation, missing data at the inshore end of the pass were infilled by repeating the nearest SLA measurement. This gave a conservative estimate of the resulting geostrophic velocity anomaly (*Geostrophic Velocity* section) as it meant there was no across-track SLA gradient. For the spatial interpolation, missing data along the track were linearly interpolated. Up to four missing data points (c. 30 km) were used for the spatial infilling as the first baroclinic Rossby radius of deformation for the region is between 20–30 km (Chelton et al. 1998) and therefore measurements over these spatial scales would be expected to be correlated for geostrophic flows. After the spatial interpolation, any remaining missing data were infilled by linear interpolation in time.

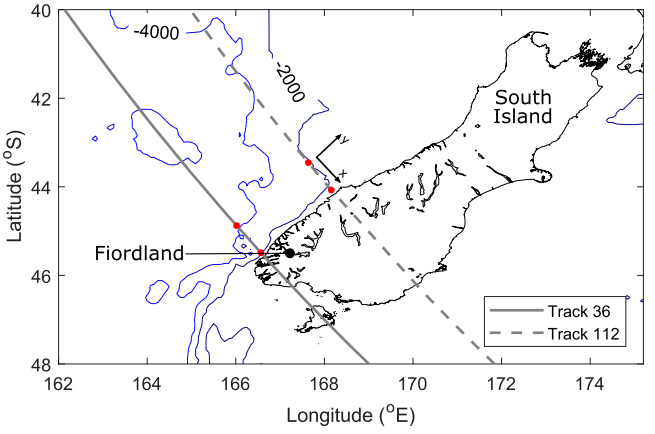

Figure 2. Satellite altimeter tracks 36 and 112. The inner and outer altimeter measurements used in the study are indicated by the red dots. Bathymetric contours are 2000m and 4000 m.

The MDT used was MDT_CNES-CLS13, referenced to 1993–2012, produced by CLS and distributed by Aviso+ with support from CNES (https://www.aviso.altimetry.fr/). MDT was linearly interpolated to the altimeter measurement locations and both SLA and MDT were re-referenced to 1993–2016. The SLA record was annually smoothed using a cosine filter over 13 months (Emery and Thomson 2001) to remove higher frequency variability, which was not of interest in the present study (*Geostrophic Velocity* section).

Geostrophic velocity

The mean across-track surface geostrophic velocity ($\overline{v_g}$) for track 36 offshore of the Fiordland coast was calculated using the MDT and time-averaged unsmoothed SLA, similar to Fernandez et al. (2018). The MDT and average SLA at each location were summed to get the average absolute dynamic topography ($\overline{ADT}$). The geostrophic velocity was then calculated by $\overline{v_g} = (g/f)(\partial\overline{ADT}/\partial x)$, where g is acceleration due to gravity, f is the Coriolis parameter, and $\partial\overline{ADT}/\partial x$ is the time-averaged along-track ADT gradient. The gradient was calculated using the gradient function in MATLAB, which takes the gradient over three points, except at the ends where the two adjacent points are used.

The mean geostrophic velocity, $\overline{v_g}$, was used to determine the offshore extent of the FC by noting that the velocity changed sign after the 11th measurement point from the coast, approximately 73.1 km offshore (Figure 3). Therefore the inshore 11 altimeter measurements were used to define the FC. There was also some structure evident in $\overline{v_g}$, with stronger velocities closer to the coast and weaker velocities further offshore. Due to this structure, an 'inner current' (the inner three altimeter measurements, 11.2–23.6 km offshore) and 'outer current' (the inner 4–11 altimeter measurements, 29.8–73.1 km offshore) were also examined.

A time-series of the across-track surface geostrophic velocity anomaly (v_g') for track 36 was calculated using the unsmoothed SLAs. The geostrophic velocity anomaly, v_g', was calculated for each data point from $v_g' = (g/f)(\partial\eta/\partial x)$, where $\partial\eta/\partial x$ is the along-track SLA

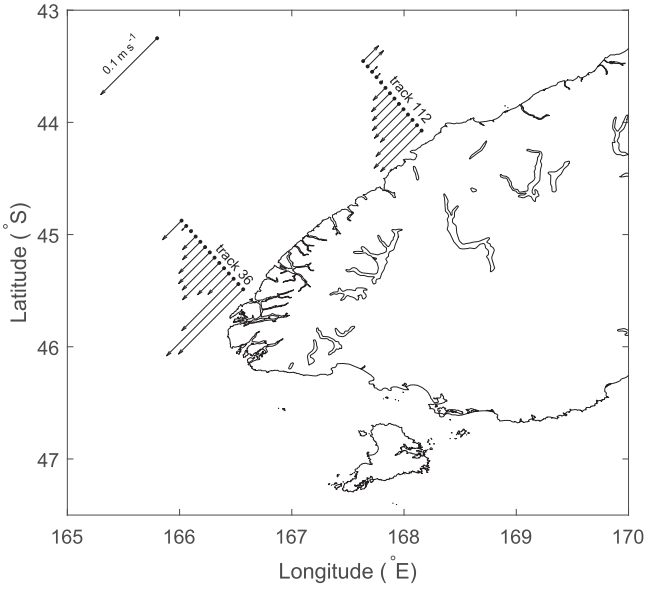

Figure 3. Mean (referenced to 1993–2016) across-track surface geostrophic current for September 1992–May 2017 offshore of the Fiordland coast for altimeter tracks 36 and 112. The maximum velocity is 0.13 m s^{-1} southwestward across track 36 and 0.08 m s^{-1} southwestward across track 112. A 0.1 m s^{-1} reference arrow is included in the top left.

gradient. A positive velocity was northeastward up the coast and a negative velocity southwestward down the coast. The geostrophic velocity anomaly, v_g', at each measurement point was annually-smoothed using a cosine filter over 13 months. To calculate v_g' over the full FC, the annually-smoothed v_g' was averaged over the 11 inshore measurements for each date. Similarly, annually-smoothed v_g' was averaged over the 3 inshore measurements for the inner current, and over inshore measurements 4–11 for the outer current. Annual smoothing was used as no clear seasonal cycles were evident (not shown) and so only interannual and longer timescales were considered.

Decadal variability has been found in the EACx using five-year smoothed fields (e.g. Ridgway 2007; Ridgway et al. 2008; Hill et al. 2011). Therefore a time-series was produced to examine decadal variability in the FC by applying a five-year smoothing to the unsmoothed v_g' for the full FC using a cosine filter over 61 months.

Alongshore SLA gradient

To examine the influence of the alongshore pressure gradient on the FC, the alongshore SLA gradient between track 36 and track 112 (an altimeter track to the north, Figure 2) was calculated. SLA data for track 112 was processed using the same methods as for track 36. Approximately 9% of SLA data was missing for track 112. The mean geostrophic velocity, $\overline{v_g}$, for track 112 was also calculated following the same methods as track 36. From $\overline{v_g}$ (Figure 3), it was evident that southwestward velocities extended out to approximately 61.0 km offshore (9 inshore measurements). The spatial structure was also evident at track 112, corresponding to the 3 inshore measurements and inshore measurements 4–9 respectively, though was not as obvious as at track 36.

To calculate the alongshore SLA gradient, the annually-smoothed track 112 SLAs were linearly interpolated to the same times as the annually-smoothed track 36 SLAs. Average SLAs for the FC at track 36 were then calculated for each date by averaging over the inshore 11 points, inshore 3 points, and inshore 4–11 points for the full, inner, and outer current respectively. For track 112, the inshore 9 points, inshore 3 points, and inshore 4–9 points were used. Alongshore SLA gradients for the full, inner, and outer current were calculated by subtracting track 36 from track 112 and dividing this by the distance between the tracks. A positive value for SLA gradient corresponds to a higher SLA in the north (track 112) than the south (track 36), which would be expected to be associated with a southwestward flow (negative v_g').

Winds and Southern Oscillation Index

Monthly zonal and meridional wind stress data for January 1958–May 2018 were downloaded from the Japanese 55-year Reanalysis (JRA-55) (Kobayashi et al. 2015). To examine potential connections between the FC and the large-scale winds, the WSC was calculated for the South Pacific region 20–50°S 180–280°E (e.g. Hill et al. 2008, 2011; Shears and Bowen 2017). This SPWSC was annually-smoothed using a cosine filter over 13 months.

To examine the influence of a more local WSC, the southeast Tasman WSC was calculated for the region 40–45°S 155–165°E. This WSC was annually-smoothed using a cosine filter over 13 months.

To examine the influence of local winds, the wind stress was averaged offshore of the Fiordland coast in a region between 44–46°S and 165–166.45°E in the south and 165–168.53°E in the north. The wind stress vector was then projected at a bearing of 33.69° onto a straight-line estimate of the Fiordland coast (between 45.6767°S 166.5038°E and 44.9529°S 167.1900°E) to obtain the alongshore wind stress. Similarly, the wind stress vector was projected at a bearing of 123.69°, normal to the coastline estimate, to obtain the cross-shore wind stress. The alongshore wind stress and cross-shore wind stress were both annually-smoothed using a cosine filter over 13 months.

Decadal variability has been found to occur in the SPWSC (e.g. Hill et al. 2011; Fernandez et al. 2018). Therefore, to examine decadal variability in the SPWSC, a time-series was calculated with a five-year smoothing using a cosine filter over 61 months.

Monthly SOI values for January 1866–April 2018 were downloaded from https://www.esrl.noaa.gov/psd/gcos_wgsp/Timeseries/SOI/, which is based on the methodology given by Ropelewski and Jones (1987). The SOI was annually-smoothed using a cosine filter over 13 months.

Correlations

Correlations were calculated between v_g' and potential drivers of the current (alongshore SLA gradient, SPWSC, southeast Tasman WSC, alongshore wind stress, and cross-shore wind stress). The SOI was also correlated with v_g' to determine if there was any correspondence between the FC and ENSO. All correlations were performed on detrended, annually-smoothed time-series.

To evaluate the statistical significance of the correlations, an Effective Degrees of Freedom (EDOF) was calculated for each detrended, annually-smoothed time-series by

auto-correlating the time-series and finding the time lag of the first zero crossing of the correlation coefficient (r). The area under the curve to this zero crossing was calculated and the integral time scale, i.e. the time for a curve with perfect correlation ($r = 1$) to have the same area, was found (Emery and Thomson 2001). The EDOF was then calculated by dividing the length of the time-series by the integral time scale. The smallest EDOF of the two time-series being correlated was used, along with the correlation coefficient (r) between the time series, to calculate the p-value of the correlation using a two-tailed t-test from Soper (2018).

Correlations and significance were also calculated between the detrended five-year smoothed v_g' and the detrended five-year smoothed SPWSC.

Significance of linear trends

To assess the significance of the linear trends, 95% confidence intervals were calculated. Confidence intervals were calculated by

$$\pm t \frac{s}{\sqrt{\sum (x_i - \bar{x})^2}},$$

where t is the t-value corresponding to the Degrees of Freedom (DOF), x_i are the x values (in this case time), and $\bar{x}$ is the mean of the x values (Draper and Smith 1998). The standard error, s, was calculated by

$$s = \sqrt{\frac{\sum e_i^2}{DOF - 2}},$$

where e_i are the residuals. t-values were obtained by referencing a t-table (http://davidmlane.com/hyperstat/t_table.html). For each variable, the DOF was the EDOF estimated previously (*Correlations* section). A linear trend was considered significant if it did not include 0 within its 95% confidence interval (Draper and Smith 1998; Emery and Thomson 2001).

Relative magnitudes of alongshore forcing

Godfrey and Ridgway (1985) used the depth integral of the alongshore momentum equation to compare the roles of the alongshore pressure gradient and alongshore wind stress in driving the LC, and a similar approach is used here. Following their notation, the depth-averaged alongshore momentum equation can be expressed as

$$\int \frac{Dv}{Dt} \, \mathrm{dz} - R + fU = -g \frac{\partial S}{\partial y} + \frac{\tau}{\rho_0}$$

Where Dv/Dt is the Lagrangian derivative (total derivative) of the alongshore velocity v, R is the depth integral of all Reynolds stress terms due to bottom stress, interfacial stress, lateral friction, and mesoscale eddy effects, f is the Coriolis parameter, U is the depth integral of the cross-shore velocity u, g is acceleration due to gravity, S is the depth-integrated steric height, y is the alongshore distance, τ is the alongshore wind stress, and ρ_0 is a reference density (Godfrey and Ridgway 1985). The forcing function of the alongshore flow can

be written as $-g(\partial S/\partial y) + (\tau/\rho_0)$ (i.e. the right-hand side of the equation). The left-hand side of the equation is not as straightforward, with the alongshore flow contributing to both the acceleration and the integral of the stress, and therefore was not evaluated. The time derivative of the geostrophic flows were calculated and found to be small and weakly correlated with all drivers considered. In the current study 1028 kg m^{-3} was used as the reference density, and depths of both 100 m (for the surface ocean) and 2000m (for the full ocean) were used for the depth-integrated steric height. Only surface height data was used for the depth-integrated steric height calculations (due to a lack of in situ data) and it is therefore assumed that the flow is barotropic. The 2000m depth was chosen because the measurements for track 112 lay approximately along the 2000m depth contour (Figure 2). Furthermore, Heath (1972) found the reference level in the Tasman Basin to be 2300 dbars but noted that weak sub-surface flows mean that a shallower reference level should not have a significant effect on surface geostrophic current calculations.

Individual forcing terms (alongshore pressure gradient, $-g(\partial S/\partial y)$, and alongshore wind stress, τ/ρ_0) and the combined forcing term (sum of the two individual terms, $-g(\partial S/\partial y) + (\tau/\rho_0)$) were calculated for both the mean and the altimeter time-series. To calculate the pressure gradient in the mean, the $\overline{ADT}$ (*Geostrophic Velocity* section) was multiplied by the depth (100 m or 2000 m) and averaged over the appropriate extent of the current. The mean depth-integrated alongshore ADT gradient was then calculated as track 112 minus track 36 divided by the distance between the tracks for the full, inner, and outer current and this was multiplied by $-g$ to obtain the pressure gradient. Similarly, to calculate the time-varying pressure gradient, the annually-smoothed SLAs along both track 36 and 112 were multiplied by the depth (100 m or 2000m) and averaged over the appropriate extent of the current at each date. The gradient of the depth-integrated SLA between track 112 and track 36 was calculated for the full, inner, and outer current at each date as track 112 minus track 36 divided by the distance between the tracks and multiplied by $-g$ to obtain the pressure gradient. Forcing terms were calculated so that a positive alongshore forcing was equatorward and a negative forcing was poleward.

Results

Mean state

The mean geostrophic velocity, $\overline{v_g}$, for the FC was found to be southwestward (poleward) along the Fiordland coast (Figure 3). The current extended approximately 73.1 km offshore, with an average velocity (from 11.2–73.1 km offshore) of 0.06 m s^{-1}. A maximum velocity of 0.13 m s^{-1} was found approximately 17.4 km offshore. Spatial structure was evident within the current, with stronger poleward velocities 11.2–23.6 km offshore. This area was therefore considered the inner current, with the current from approximately 29.8–73.1 km offshore considered the outer current. The mean flow in the inner current was 0.11 m s^{-1} poleward and the mean flow in the outer current was 0.05 m s^{-1} poleward.

Interannual variability

The annually-smoothed time-series of v_g' were dominated by interannual variability (Figure 4). Large interannual variability was also evident in possible drivers of the

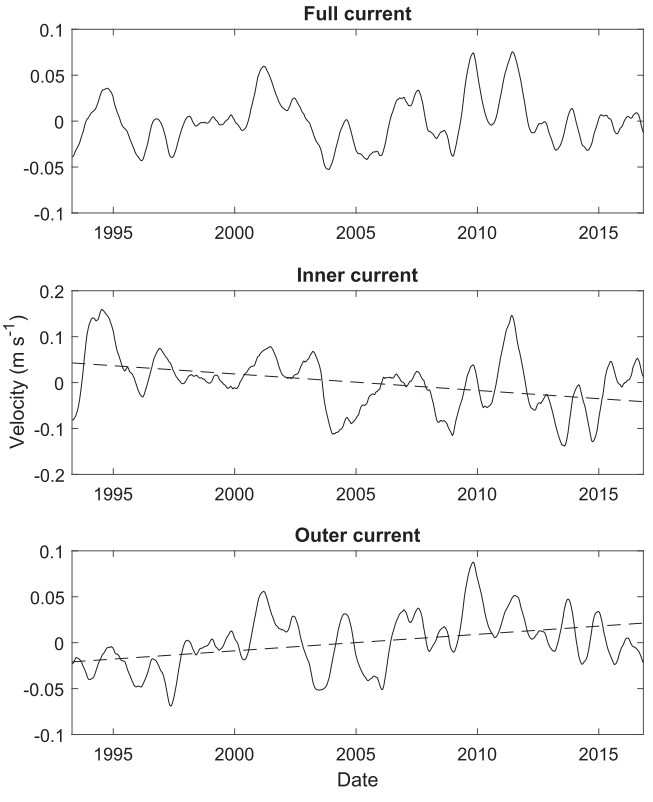

Figure 4. Annually-smoothed, across-track, surface geostrophic velocity anomalies (m s^{-1}) for the full Fiordland Current (top), inner Fiordland Current (middle), and outer Fiordland Current (bottom) over the altimeter record (April 1993–November 2016). Linear trends are shown as dashed lines where significant at the 95% confidence interval (full current = $0.33 \pm 1.11 \times 10^{-2}$ m s^{-1} $decade^{-1}$, inner current = $-3.59 \pm 2.31 \times 10^{-2}$ m s^{-1} $decade^{-1}$, outer current = $1.79 \pm 1.24 \times 10^{-2}$ m s^{-1} $decade^{-1}$). Negative values represent a poleward anomaly.

current (Figures 5 and 6). In general, v_g' was weakly correlated ($|r| < 0.3$) with the drivers examined, including the SOI (Table 1). However, statistically significant ($P < 0.05$) correlations were found between v_g' over the inner current and the alongshore SLA gradient for the inner current ($r = 0.33$), and between v_g' over the full current and the alongshore wind stress ($r = 0.30$). The signs of these correlations indicate that when the alongshore SLA gradient slopes downward to the northeast (southwest) the poleward geostrophic velocity increases (decreases), and when the alongshore wind stress is poleward (equatorward) the poleward geostrophic velocity increases (decreases).

Alongshore forcing

In the mean, the alongshore pressure gradient was the dominant forcing term for both depths of integration considered (100 m and 2000 m, Table 2). The negative values for the alongshore pressure gradient indicate a poleward alongshore pressure gradient (sloping downward to the southwest) while the positive values for the alongshore wind correspond to an equatorward alongshore wind. As the combined forcing is negative, the combination

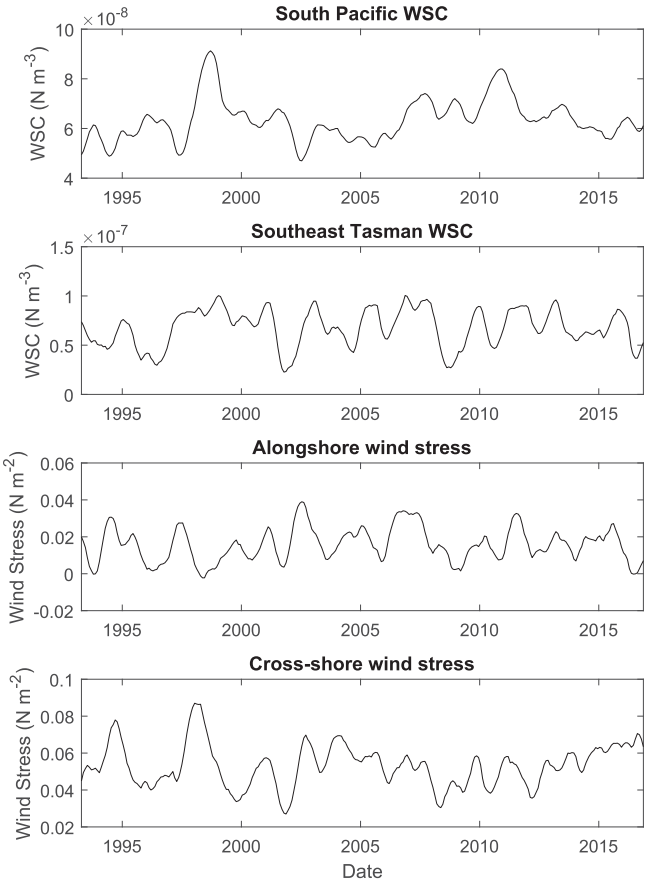

Figure 5. Annually-smoothed South Pacific (180–280°E 20–50°S) wind stress curl (WSC, N m^{-3}, top), southeast Tasman (155–165°E 40–45°S) WSC (N m^{-3}, middle), and alongshore and cross-shore wind stresses (N m^{-2}, calculated over the region 44–46°S and 165–166.45°E in the south and 165–168.53°E in the north, bottom) over the altimeter record (April 1993–November 2016). Linear trends are not significant at the 95% confidence interval (South Pacific WSC = $2.19 \pm 4.69 \times 10^{-9}$ N m^{-3} $decade^{-1}$, southeast Tasman WSC = $2.65 \pm 7.25 \times 10^{-9}$ N m^{-3} $decade^{-1}$, alongshore wind stress = $1.31 \pm 3.33 \times 10^{-3}$ N m^{-2} $decade^{-1}$, cross-shore wind stress = $0.47 \pm 4.71 \times 10^{-3}$ N m^{-2} $decade^{-1}$). A positive alongshore wind stress is equatorward. A positive cross-shore wind stress is toward the coast.

of these two terms drives a poleward flow. This is in agreement with the mean poleward geostrophic flow observed for the FC (Figure 3). At interannual time-scales, the pressure gradient forcing again dominated for both depths of integration (100 m, Figure 7, and 2000 m, not shown). Correlations were not carried out between the combined forcing time-series and v_g' as the alongshore forcing was dominated by the alongshore pressure gradient, and the alongshore SLA gradient had already been correlated with v_g' (Table 1).

Decadal variability

Decadal variability was evident in the FC, with maximum equatorward v_g' in 2001 and 2010 and maximum poleward v_g' in 1997, 2004, and 2014 (Figure 8). A statistically

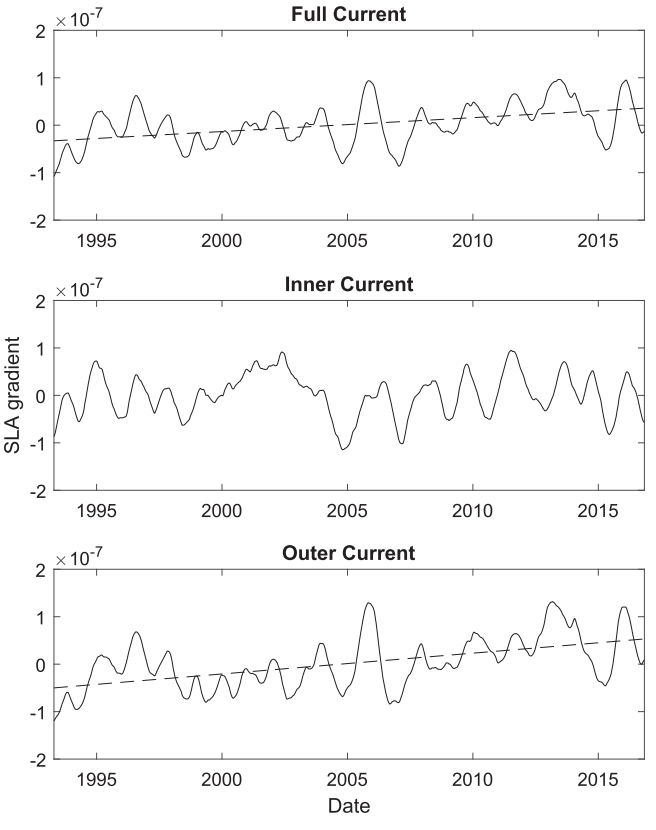

Figure 6. Annually-smoothed alongshore sea-level anomaly (SLA) gradient between the northern altimeter track (112) and the southern altimeter track (36) for the full Fiordland Current (top), inner Fiordland Current (middle), and outer Fiordland Current (bottom) over the altimeter record (April 1993–November 2016). Linear trends are shown as dashed lines where significant at the 95% confidence interval (full current = $2.92 \pm 1.41 \times 10^{-8}$ decade^{-1}, inner current = $0.23 \pm 1.63 \times 10^{-8}$ decade^{-1}, outer current = $4.38 \pm 1.76 \times 10^{-8}$ decade^{-1}). A positive value corresponds to a SLA gradient with higher SLA in the northeast than the southwest.

significant correlation was found between v_g' and the SPWSC ($r = 0.62$, $P < 0.05$). The positive correlation suggests that when the SPWSC increases, the poleward geostrophic velocity in the FC weakens. The variability appeared to be in phase in the recent time-series, but slightly out-of-phase earlier in the time-series (maximums in the five-year smoothed SPWSC in 1999 and 2010, and minimums in 1992 (not shown), 2004, and 2015) (Figure 8).

Longer-term trends

No significant trend was evident in the annually-smoothed v_g' for the full extent of the FC. However, statistically significant trends were evident within the current, with a negative trend in the inner current and a positive trend in the outer current (Table 3, Figure 4). As the FC has a mean poleward geostrophic flow (negative velocity, Figure 3), these trends indicate that the inner current has strengthened and the outer current weakened

Table 1. Correlation coefficients (*r*), *p*-values (*P*), and Effective Degrees of Freedom (EDOF) for correlations between the detrended, annually-smoothed, across-track, surface geostrophic velocity anomaly (for the full, inner, and outer current) and the alongshore sea-level anomaly gradient (SLA gradient), the South Pacific wind stress curl (SPWSC), the southeast Tasman wind stress curl (SE Tas WSC), the alongshore wind stress (Along WS), the cross-shore wind stress (Cross WS), and the Southern Oscillation Index (SOI).

Driver	Current	*r*	*P*	EDOF
SLA gradient	Full	−0.05	0.750	51
	Inner*	0.33	0.015	55
	Outer	−0.22	0.155	43
SPWSC	Full	0.21	0.255	30
	Inner	0.00	0.990	30
	Outer	0.29	0.122	30
SE Tas WSC	Full	0.20	0.168	51
	Inner	0.16	0.256	55
	Outer	0.14	0.366	43
Along WS	Full*	0.30	0.030	51
	Inner	0.20	0.138	55
	Outer	0.25	0.106	43
Cross WS	Full	0.06	0.678	51
	Inner	0.16	0.250	52
	Outer	−0.05	0.756	43
SOI	Full	0.12	0.480	37
	Inner	−0.04	0.816	37
	Outer	0.19	0.250	37

Starred (*) drivers indicate statistically significant correlations.

Table 2. Mean pressure gradient forcing ($-g(\partial S/\partial y)$, $m^2\ s^{-2}$), alongshore wind stress forcing (τ/ρ_0, $m^2\ s^{-2}$), and the sum of the two ($-g(\partial S/\partial y) + (\tau/\rho_0)$, $m^2\ s^{-2}$) for the full, inner, and outer Fiordland Current over the altimeter record (April 1993–November 2016).

Current	Depth Integration (m)	Pressure Gradient ($m^2\ s^{-2}$)	Alongshore Wind ($m^2\ s^{-2}$)	Combined Forcing ($m^2\ s^{-2}$)
Full	100	-1.08×10^{-4}	1.53×10^{-5}	-9.31×10^{-5}
	2000	-2.17×10^{-3}		-2.15×10^{-3}
Inner	100	-7.75×10^{-5}	1.53×10^{-5}	-6.22×10^{-5}
	2000	-1.55×10^{-3}		-1.53×10^{-3}
Outer	100	-1.14×10^{-4}	1.53×10^{-5}	-9.84×10^{-5}
	2000	-2.27×10^{-3}		-2.26×10^{-3}

Negative (positive) values represent a poleward (equatorward) forcing.

over the altimeter record, with the net result being no significant change in the strength of the overall current. Significant positive trends were only identified in the alongshore SLA gradient for both the full and outer FC, whilst linear trends in all other drivers were not statistically significant (Table 3, Figures 5 and 6).

Discussion

The mean geostrophic flow in the FC was found to be poleward (Figure 3), agreeing with previous studies (Brodie 1960; Heath 1973; Stanton 1976; Stanton and Moore 1992; Moore and Murdoch 1993). This mean flow is consistent with the mean poleward alongshore pressure gradient, which is substantially larger than the mean equatorward alongshore wind stress (Table 2). This result agrees with Ridgway and Dunn (2003), who hypothesised that the FC was driven by the alongshore pressure gradient which opposes the alongshore wind stress, and also suggests that the mean flow in the FC is primarily driven by the same

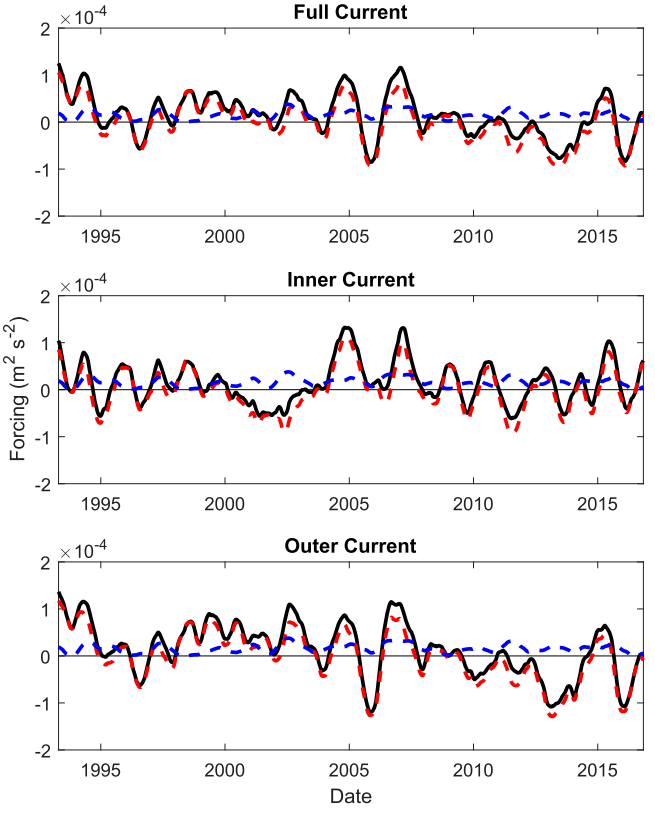

Figure 7. Annually-smoothed alongshore pressure gradient anomaly ($-g(\partial S/\partial y)$, red dashed line), alongshore wind stress (τ/ρ_0, blue dashed line), and combined ($-g(\partial S/\partial y) + (\tau/\rho_0)$, solid black line) forcing terms ($m^2\ s^{-2}$) integrated over the upper ocean (100 m) for the full (top), inner (middle), and outer (bottom) Fiordland Current over the altimeter record (April 1993–November 2016). Negative values represent a poleward forcing.

Table 3. Linear trends in the geostrophic velocity of the Fiordland Current and its potential drivers over the altimeter record (April 1993–November 2016) with 95% confidence intervals (95% CI).

Variable	Trend	95% CI
Full geostrophic velocity	0.33×10^{-2}	$\pm 1.11 \times 10^{-2}$
Inner geostrophic velocity*	-3.59×10^{-2}	$\pm 2.31 \times 10^{-2}$
Outer geostrophic velocity*	1.79×10^{-2}	$\pm 1.24 \times 10^{-2}$
SPWSC	2.19×10^{-9}	$\pm 4.69 \times 10^{-9}$
SE Tas WSC	2.65×10^{-9}	$\pm 7.25 \times 10^{-9}$
Alongshore WS	1.31×10^{-3}	$\pm 3.33 \times 10^{-3}$
Cross-shore WS	0.47×10^{-3}	$\pm 4.71 \times 10^{-3}$
Full SLA gradient*	2.92×10^{-8}	$\pm 1.41 \times 10^{-8}$
Inner SLA gradient	0.23×10^{-8}	$\pm 1.63 \times 10^{-8}$
Outer SLA gradient*	4.38×10^{-8}	$\pm 1.76 \times 10^{-8}$

Trends are in units of m s^{-1} $decade^{-1}$ for the full, inner, and outer geostrophic velocity; N m^{-3} $decade^{-1}$ for the South Pacific wind stress curl (SPWSC) and southeast Tasman wind stress curl (SE Tas WSC); N m^{-2} $decade^{-1}$ for the alongshore and cross-shore wind stress (WS); and $decade^{-1}$ for the full, inner, and outer alongshore sea-level anomaly gradient (SLA gradient). A negative velocity trend represents increased poleward flow, a positive wind stress curl trend represents increased wind stress curl, a positive alongshore WS trend represents increased equatorward wind stress, a positive cross-shore WS trend represents increased wind stress toward the coast, a positive SLA gradient trend represents increased higher SLA in the northeast compared to the southwest. Starred (*) variables indicate trends significant at the 95% CI.

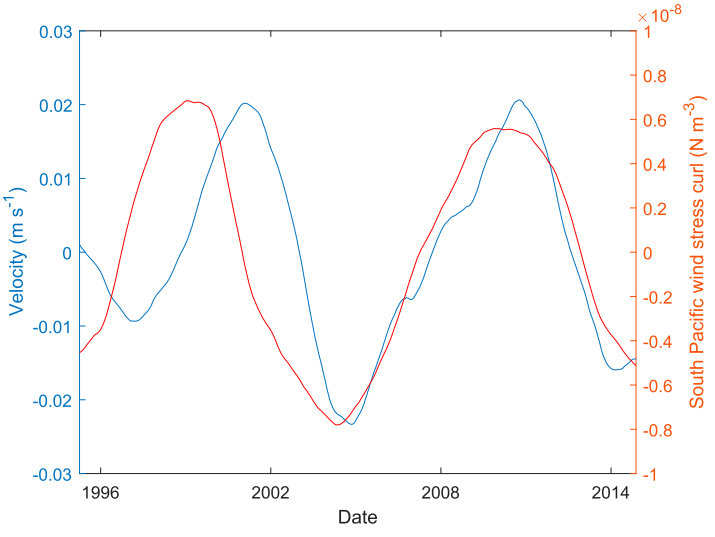

Figure 8. Detrended, five-year smoothed, across-track, surface geostrophic velocity anomaly (m s^{-1}) for the full Fiordland Current (blue) and detrended, five-year smoothed South Pacific (180–280°E 20–50°S) wind stress curl (N m^{-3}, red) over the altimeter record (April 1995–November 2014). Negative velocities represent a poleward anomaly. The correlation between the time-series is $r = 0.62$, $P = 0.032$, EDOF = 12.

factors as the mean flow in the LC (Godfrey and Ridgway 1985; Morrow and Birol 1998; Feng et al. 2003; Ridgway and Condie 2004). The mean geostrophic velocity structure in the FC, with the strongest velocities near the coast and a general decrease in velocity offshore, is consistent with earlier hydrographic surveys (Heath 1973; Stanton 1976).

Although the mean geostrophic flow in the FC is consistent with the alongshore pressure gradient, at interannual time-scales, variability in the geostrophic velocity was only weakly correlated with the alongshore SLA gradient (Table 1). However, a significant correlation was found between interannual variability in the FC and the alongshore wind stress. This correlation was positive, indicating that an equatorward alongshore wind stress leads to a decreased poleward geostrophic velocity in the FC. Chiswell (1996) also found that variability in the inshore portion of the SC, which transports mainly STW (Sutton 2003), was strongly correlated to the winds over southern New Zealand. These results therefore suggest that local winds may be important in driving variability in STW transport around southern New Zealand.

A significant correlation was also found between interannual variability in the inner current and the alongshore SLA gradient (Table 1). However, this correlation was positive, indicating that as the southwestward downsloping SLA gradient weakens, the poleward geostrophic velocity increases. This result is unexpected, with no clear dynamical explanation. Although it is possible that errors have been introduced by the extrapolation of missing data near the coast, this extrapolation is unlikely to have reversed the tendency of the geostrophic flow on interannual time scales. It is also noted that the alongshore gradient was calculated between two altimeter tracks, and these tracks may be further apart than the scale of the alongshore pressure gradients that drive interannual variability in the flow at track 36. Stanton (1976) found that the FC strengthens

where the continental slope steepens around 44°S (which is roughly the location of the northern altimeter track used here, Figure 2), whereas it is fully developed further south along the Fiordland coast. This location (44°S) is also the approximate location where STW bifurcates into equatorward and poleward flows on the West Coast (Heath 1975; Stevens et al. 2019), although the latitudinal range varies in the literature (Heath 1973, 1975; Stanton and Moore 1992). Overall, the large interannual variability evident in the FC is consistent with the high interannual variability found by Fernandez et al. (2018) in New Zealand WBCs.

Decadal variability was evident in the FC and was found to be significantly correlated with decadal variability in the SPWSC (Figure 8). This correlation was positive, indicating that as the SPWSC increases, the poleward geostrophic velocity decreases, which is consistent with the response of a traditional EBC (i.e. increased equatorward transport under stronger WSC) (Sverdrup 1947). However, the short time-series means that there are only two quasi-decadal cycles present. Quasi-decadal variability has also been found in the EACx (Ridgway 2007; Hill et al. 2008; Ridgway et al. 2008). Ridgway (2007) reported that temperature and salinity at Maria Island, Tasmania had a minimum in the mid-1990s then increased to the early 2000s, suggesting a decrease and increase in EACx transport respectively. Consistent with this, Ridgway et al. (2008) observed a weakening of transport in the mid-1990s and a maximum in 2000/2001. In comparison, decadal variability in the FC demonstrated an increased poleward geostrophic velocity in 1997 and a weaker poleward geostrophic velocity in 2001, roughly opposing the changes in the EACx. Fernandez et al. (2018) also found that, in general, weaker surface transports were observed in New Zealand's subtropical WBCs at times of larger SPWSC, consistent with the FC. In the case of the New Zealand subtropical WBCs, this weaker transport may be related to reduced transport through the TF (Hill et al. 2011). However, changes in the transport of the TF would not be expected to directly influence the FC as there is no clear pathway between the two (Figure 1) (Ridgway and Dunn 2003).

Significant trends were evident in the inner and outer FC, with the outer current demonstrating a weakening trend and the inner current demonstrating a strengthening trend (Figure 4). No significant trend was found in the full FC, consistent with Fernandez et al. (2018) who found no significant trends in the transport of New Zealand WBCs over the altimeter record. Of the possible drivers considered, significant trends were only present in the alongshore SLA gradient for the full and outer current (Table 3). These trends indicate that the poleward alongshore gradient has increased, which would be expected to be associated with increased poleward flow, yet a weakening trend is seen in the outer FC. As has been discussed earlier, this may be because the distance between the altimeter tracks used to calculate the alongshore gradient is at a larger scale than the alongshore pressure gradient that drives variability at the altimeter line considered here.

The weakening poleward trend in the outer current is consistent with the response of a traditional EBC to gyre spin-up due to increased WSC, as has been seen in the South Pacific subtropical gyre (Roemmich et al. 2007, 2016). However, no significant trend in the SPWSC was found over the altimeter record (Table 3). Other studies (e.g. Hill et al. 2008; Shears and Bowen 2017) have found increasing trends in the SPWSC since the 1950s and a significant positive trend in the SPWSC was also found in the present

study for July 1958–November 2017, suggesting that the non-significant trend may be due to the short time-series and reduced EDOF. A possible relationship between an increasing SPWSC and weakening poleward flow is supported by the correlation between decadal variability in the FC and decadal variability in the SPWSC (Figure 8).

The inner current demonstrates a strengthening poleward trend, opposite to the weakening trend in the outer FC. This suggests that different dynamics may be impacting on the inshore section of the current. Freshwater inflow along the Fiordland coast could establish a poleward flowing EBC through buoyancy forcing (Gill 1982), as the Fiordland region experiences high rainfall and freshwater run-off (Stanton and Pickard 1981), with Stanton (1976), Butler et al. (1992), and Smith et al. (2013) finding low salinities close to the coast and strong salinity gradients moving offshore. To briefly examine the relationship between freshwater inflow and the inner FC, monthly rainfall data for Puysegur Point (46.156°S 166.613°E, January 1991–June 2018) and Secretary Island (45.221°S 166.886°E, January 1994–January 2018) were downloaded from the New Zealand National Climate Database (https://cliflo.niwa.co.nz/). Rainfall demonstrated a significant decreasing trend at Secretary Island and a non-significant trend at Puysegur Point (Figure 9), suggesting that changes in freshwater inflow are unlikely to be driving the long-term changes in the inner current. No significant correlations were found between interannual variability in the inner current and Puysegur Point rainfall ($r = -0.05$, $P = 0.716$) or Secretary Island rainfall ($r = -0.13$, $P = 0.388$). Input from rivers and the Manapouri power station tail-race at Doubtful Sound are also significant freshwater inputs, with input from the tail-race controlled by electricity generating requirements rather than rainfall in the Fiordland region (Stanton and Pickard 1981). However, an estimate of the total freshwater input over the region is beyond the scope of this study.

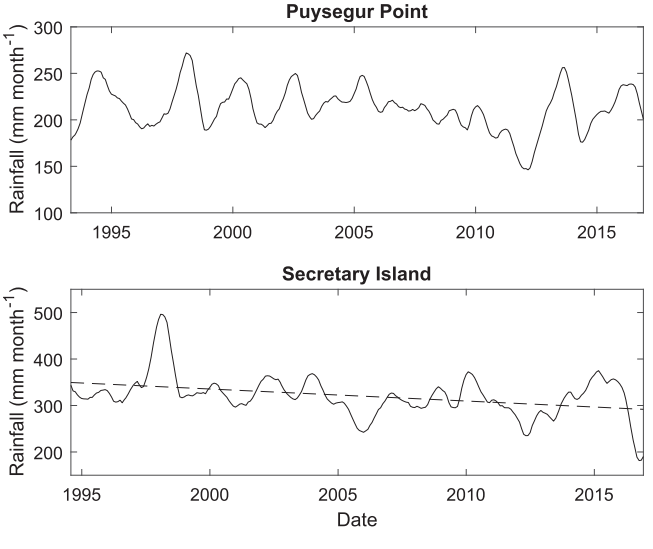

Figure 9. Annually-smoothed rainfall (mm month^{-1}) for Puysegur Point (April 1993–November 2016, top) and Secretary Island (July 1994–November 2016, bottom). Linear trends are shown as dashed lines where significant at the 95% confidence interval (Puysegur Point = -7.87 ± 8.78 mm month^{-1} decade^{-1}, Secretary Island = -25.85 ± 19.85 mm month^{-1} decade^{-1}). Note the different time-scales on the x-axis.

Conclusions

This study has demonstrated that the mean alongshore geostrophic flow in the FC is poleward, with the mean current extending approximately 73.1 km offshore. Spatial structure has led to an inner current (11.2–23.6 km offshore) and outer current (29.8–73.1 km offshore) being considered. In the mean, the alongshore momentum equation is dominated by the poleward alongshore pressure gradient, which is substantially larger than the equatorward alongshore wind stress. It is therefore suggested that the mean poleward flow in the FC is driven by the mean poleward alongshore pressure gradient.

Large interannual variability was seen in the geostrophic velocity of the FC, however correlations with interannual variability in most of the drivers considered were not statistically significant. A significant correlation was found between the alongshore wind stress and the FC, suggesting that an equatorward (poleward) alongshore wind stress results in reduced (increased) poleward geostrophic velocity. However, as none of the correlations were strong, the FC may be influenced by a number of factors, with no single driver dominant at interannual time-scales.

Decadal variability was also seen in the geostrophic velocity of the FC, and this was significantly correlated with decadal variability in the SPWSC. This correlation indicates that as the SPWSC increases (decreases) the poleward geostrophic velocity in the FC decreases (increases), which is consistent with the response of a traditional EBC.

Longer-term trends in the geostrophic velocity of the FC were found to be statistically significant, with the inner current strengthening and the outer current weakening. The net result was a non-significant trend in the full FC. Trends in the SPWSC, southeast Tasman WSC, cross-shore wind stress, and alongshore wind stress were found to be non-significant, although the SPWSC demonstrates a significant increasing trend over longer time-periods.

The correlation between decadal variability in the FC and the SPWSC, and the trend in the outer FC, are consistent with the dynamics of a traditional EBC and suggest that, on decadal and longer time-scales, a stronger SPWSC may lead to reduced poleward flow in the FC. The trend in the inner FC opposes that of the outer FC, suggesting that the inner current may be controlled by different dynamics.

Future work could compare variability in the FC with that in the EAC/EACx as it is possible that some of the STW transported in the EAC exits the Tasman Sea along the southwest coast of New Zealand (Ridgway and Dunn 2003). It would also be of interest to examine where water transported in the FC ends up to highlight areas affected by changes in the FC. Increased transport in the inner FC could lead to warming and 'tropicalisation' (i.e. increased proportion of tropical species) (Ling et al. 2009; Shears and Bowen 2017; Fowler et al. 2018), with Sutton and Bowen (2019) finding SST warming trends of around 0.16–0.18°C decade^{-1} along the Fiordland Coast, and trends as large as 0.22°C decade^{-1} around Southern New Zealand. Furthermore, an array of current meters could be located along the altimeter track to compare in situ observations with the geostrophic velocities calculated from the altimeter data. This would be useful to validate the altimeter-derived velocities as well as the interpolation and extrapolation methods used in the present study and, if measurements were also taken at depth, transport in the FC could be estimated.

Acknowledgements

The sea-level anomaly (SLA) altimeter products used in this study were produced and distributed by the Copernicus Marine Environment Monitoring Service (http://www.marine.copernicus.eu). The mean dynamic topography (MDT) product was produced by CLS and distributed by Aviso+, with support from CNES (https://www.aviso.altimetry.fr/). The wind stress data is from the Japanese 55-year Reanalysis (JRA-55) carried out by the Japan Meteorological Agency. The Southern Oscillation Index (SOI) data is from the Climatic Research Unit, University of East Anglia, with the data hosted by the National Oceanic and Atmospheric Administration (https://www.esrl.noaa.gov/psd/gcos_wgsp/Timeseries/SOI/). The rainfall data is from the National Institute of Water and Atmospheric Research (https://cliflo.niwa.co.nz/). M. C. acknowledges the support of a University of Auckland Postgraduate Honours Scholarship. The authors also thank two anonymous reviewers for their comments which helped improve the manuscript.

Disclosure statement

No potential conflict of interest was reported by the authors.

References

Brodie JW. 1960. Coastal surface currents around New Zealand. New Zealand Journal of Geology and Geophysics. 3(2):235–252.

Butler ECV, Butt JA, Lindstrom E, Teldesley P, Pickmere S, Vincent W. 1992. Oceanography of the subtropical Convergence Zone around southern New Zealand. New Zealand Journal of Marine and Freshwater Research. 26(2):131–154.

Cahill ML, Middleton JH, Stanton BR. 1991. Coastal-trapped waves on the west coast of South Island, New Zealand. Journal of Physical Oceanography. 21:541–557.

Cai W. 2006. Antarctic ozone depletion causes an intensification of the Southern Ocean supergyre circulation. Geophysical Research Letters. 33:L03712.

Chelton DB, deSzoeke RA, Schlax MG, Naggar KE, Siwertz N. 1998. Geographical variability of the first baroclinic Rossby radius of deformation. Journal of Physical Oceanography. 28:433–460.

Chiswell SM. 1996. Variability in the Southland current, New Zealand. New Zealand Journal of Marine and Freshwater Research. 30(1):1–17.

Chiswell SM, Bostock HC, Sutton PJH, Williams MJM. 2015. Physical oceanography of the deep seas around New Zealand: a review. New Zealand Journal of Marine and Freshwater Research. 49(2):286–317.

Cortese G, Dunbar GB, Carter L, Scott G, Bostock HC, Bowen MM, Crundwell M, Hayward BW, Howard W, Martínez JI, et al. 2013. Southwest Pacific Ocean response to a warmer world: insights from marine Isotope Stage 5e. Paleoceanography. 28:585–598.

Draper NR, Smith H. 1998. Applied regression analysis, 3rd ed. New York, NY: John Wiley & Sons.

Emery WJ, Thomson RE. 2001. Data analysis methods in physical oceanography, 2nd ed. Amsterdam: Elsevier.

Feng M, Meyers G, Pearce A, Wijffels S. 2003. Annual and interannual variations of the Leeuwin current at 32°S. Journal of Geophysical Research. 108(C11):3355.

Feng M, Wijffels S, Godfrey S, Meyers G. 2005. Do eddies play a role in the momentum balance of the Leeuwin current? Journal of Physical Oceanography. 35:964–975.

Fernandez D, Bowen MM, Sutton PJH. 2018. Variability, coherence and forcing mechanisms in the New Zealand ocean boundary currents. Progress in Oceanography. 165:168–188.

Fowler AM, Parkinson K, Booth DJ. 2018. New poleward observations of 30 tropical reef fishes in temperate southeastern Australia. Marine Biodiversity. 48(4):2249–2254.

Gill AE. 1982. Atmosphere-ocean dynamics. New York, NY: Academic Press.

Godfrey JS, Ridgway KR. 1985. The large-scale environment of the poleward-flowing Leeuwin current, western Australia: longshore steric height gradients, wind stresses and geostrophic flow. Journal of Physical Oceanography. 15:481–495.

Hamilton LJ. 2006. Structure of the subtropical Front in the Tasman Sea. Deep Sea Research Part I: Oceanographic Research Papers. 53:1989–2009.
Heath RA. 1972. Choice of reference surface for geostrophic currents around New Zealand. New Zealand Journal of Marine and Freshwater Research. 6(1-2):148–177.
Heath RA. 1973. Direct measurements of coastal currents around southern New Zealand. New Zealand Journal of Marine and Freshwater Research. 7(4):331–367.
Heath RA. 1975. Oceanic circulation and hydrology off the southern half of South Island. New Zealand. Wellington: New Zealand Department of Scientific and Industrial Research. New Zealand Oceanographic Institute Memoir 72.
Heath RA. 1982. What drives the mean circulation on the New Zealand west coast continental shelf? New Zealand Journal of Marine and Freshwater Research. 16(2):215–226.
Heath RA. 1985. Large-scale influence of the New Zealand seafloor topography on western boundary currents of the South Pacific Ocean. Marine and Freshwater Research. 36:1–14.
Hill KL, Rintoul SR, Coleman R, Ridgway KR. 2008. Wind forced low frequency variability of the east Australia current. Geophysical Research Letters. 35:L08602.
Hill KL, Rintoul SR, Ridgway KR, Oke PR. 2011. Decadal changes in the South Pacific western boundary current system revealed in observations and ocean state estimates. Journal of Geophysical Research. 116:C01009.
Hopkins J, Shaw A, Challenor P. 2010. The Southland Front. New Zealand: variability and ENSO correlations. Continental Shelf Research. 30:1535–1548.
Kobayashi S, Ota Y, Harada Y, Ebita A, Moriya M, Onoda H, Onogi K, Kamahori H, Kobayashi C, Endo H, et al. 2015. The JRA-55 reanalysis: general specifications and basic characteristics. Journal of the Meteorological Society of Japan. 93:5–48.
Ling SD, Johnson CR, Ridgway KR, Hobday AJ, Haddon M. 2009. Climate-driven range extension of a sea urchin: inferring future trends by analysis of recent population dynamics. Global Change Biology. 15:719–731.
Moore MI, Murdoch RC. 1993. Physical and biological observations of coastal squirts under non-upwelling conditions. Journal of Geophysical Research. 98(C11):20043–20061.
Morrow R, Birol F. 1998. Variability in the southeast Indian ocean from altimetry: forcing mechanisms for the Leeuwin current. Journal of Geophysical Research: Oceans. 103(C9):18529–18544.
Ridgway KR. 2007. Long-term trend and decadal variability of the southward penetration of the east Australian current. Geophysical Research Letters. 34:L13613.
Ridgway KR, Coleman RC, Bailey RJ, Sutton PJH. 2008. Decadal variability of east Australian current transport inferred from repeated high-density XBT transects, a CTD survey and satellite altimetry. Journal of Geophysical Research. 113:C08039.
Ridgway KR, Condie SA. 2004. The 5500-km-long boundary flow off western and southern Australia. Journal of Geophysical Research. 109:C04017.
Ridgway KR, Dunn JR. 2003. Mesoscale structure of the mean east Australian current system and its relationship with topography. Progress in Oceanography. 56:189–222.
Roemmich D, Gilson J, Davis R, Sutton PJH, Wijffels S, Riser S. 2007. Decadal spinup of the South Pacific subtropical gyre. Journal of Physical Oceanography. 37:162–173.
Roemmich D, Gilson J, Sutton PJH, Zilberman N. 2016. Multidecadal change of the South Pacific gyre circulation. Journal of Physical Oceanography. 46:1871–1883.
Ropelewski CF, Jones PD. 1987. An extension of the Tahiti–darwin southern Oscillation Index. Monthly Weather Review. 115:2161–2165.
Shears NT, Bowen MM. 2017. Half a century of coastal temperature records reveal complex warming trends in western boundary currents. Scientific Reports. 7:14527.
Smith RO, Vennell R, Bostock HC, Williams MJ. 2013. Interaction of the subtropical front with topography around southern New Zealand. Deep Sea Research Part I: Oceanographic Research Papers. 76:13–26.
Soper DS. 2018. *P*-value calculator for correlation coefficients. [Software]. https://www.danielsoper.com/statcalc/calculator.aspx?id=44.

Stanton BR. 1976. Circulation and hydrology off the west coast of the South Island, New Zealand. New Zealand Journal of Marine and Freshwater Research. 10(3):445–467.
Stanton BR. 2001. Estimating the east Auckland current transport from model winds and the island rule. New Zealand Journal of Marine and Freshwater Research. 35(3):531–540.
Stanton BR, Moore MI. 1992. Hydrographic observations during the Tasman boundary experiment off the west coast of South Island, New Zealand. New Zealand Journal of Marine and Freshwater Research. 26(3-4):339–358.
Stanton BR, Pickard GL. 1981. Physical oceanography of the New Zealand fiords. Wellington: New Zealand Department of Scientific and Industrial Research. New Zealand Oceanographic Institute Memoir 88.
Stevens CL, O'Callaghan JM, Chiswell SM, Hadfield MG. 2019. Physical oceanography of New Zealand/aotearoa shelf seas – a review. New Zealand Journal of Marine and Freshwater Research. 1–40.
Stramma L, Peterson RG, Tomczak M. 1995. The South Pacific current. Journal of Physical Oceanography. 25:77–91.
Sutton PJH. 2003. The Southland current: a subantarctic current. New Zealand Journal of Marine and Freshwater Research. 37(3):645–652.
Sutton PJH, Bowen MM. 2011. Currents off the west coast of Northland, New Zealand. New Zealand Journal of Marine and Freshwater Research. 45(4):609–624.
Sutton PJH, Bowen MM. 2019. Ocean temperature change around New Zealand over the last 36 years. New Zealand Journal of Marine and Freshwater Research. 1–22.
Sverdrup HU. 1947. Wind-driven currents in a baroclinic ocean; with application to the equatorial currents of the eastern Pacific. Proceedings of the National Academy of Sciences. 33(11):318–326.
Taburet G. 2018. Quality information document: sea level TAC-DUACS products. Europe: Copernicus Marine Environment Monitoring Service. [accessed 2018 May 03]. http://cmems-resources.cls.fr/documents/QUID/CMEMS-SL-QUID-008-032-051.pdf.